Plasmonic Response of Ag- and Au-Infiltrated Cross-Linked Lysozyme Crystals

Otto L. Muskens, Matt W. England, Lefteris Danos, Mei Li, and Stephen Mann**

Metal-infiltrated protein crystals form a novel class of bio-nanomaterials of great interest for applications in biomedicine, chemistry, and optoelectronics. As yet, very little is known about the internal structure of these materials and the interconnectivity of the metallic network. Here, the optical response of individual Au- and Ag-infiltrated cross-linked lysozyme crystals is investigated using angle- and polarization-dependent spectroscopy. The measurements unequivocally show that metallic inclusions formed inside the nanoporous solvent channels do not connect into continuous nanowires, but rather consist of ensembles of isolated spheroidal nanoclusters with aspect ratios as high as a value of four, and which exhibit a pronounced plasmonic response that is isotropic on a macroscopic length scale. Fluorescence measurement in the visible range show a strong contribution from the protein host, which is quenched by the Au inclusions, and a weaker contribution attributed to the molecule-like emission from small Au-clusters.

1. Introduction

Nanoporous organic-inorganic bio-nanomaterials are of considerable interest because their biocompatible, chemical, and physical properties are relevant for diverse applications in catalysis, gas storage, nanomedicine and optoelectronics.[1–4] Organic and biological molecules such as proteins and peptides can be arranged into a wide range of adaptable porous materials.[3–9] Recent work has investigated the growth of noble metal clusters both in pristine and cross-linked protein crystals following various different procedures.[6–11] Low densities of spheroidal nanoparticles were found using transmission electron microscopy (TEM) analysis in several types of organic crystals,[6,7] possibly associated with the selective nucleation of nanometer-sized Au clusters at specific positions in the protein template.[7] In contrast, soaking cross-linked tetragonal lysozyme crystals (CLLCs) in a Ag(I) aqueous solution followed by photoreduction, or in sodium borohydride followed by washing and addition of a Au(III) complex, produced well defined protein single crystals that contained significant weight percentages of metallic Ag or Au (ca. 10 wt% and 23 wt%, respectively).[8] Significantly, the metallic inclusions were nucleated specifically within the 1–2.5 nm-sized intracrystalline solvent channels such that they were periodically arranged along the crystallographic *c* axis to produce intact single crystals with a highly organized hybrid superstructure. TEM investigations showed continuous electron dense striations, ca. 2 nm in thickness, suggesting that nanofilaments of Au or Ag were assembled within the solvent channels.[8] However, because the TEM images represent 2D projections of a 3D structure, it remained unclear whether the lattice fringes were associated with a regularly spaced array of continuous metallic nanowires or whether they originated from the superimposition of discrete metallic clusters nucleated within the solvent channels. To address this ambiguity, here we present an optical characterization of individual cross-linked lysozyme crystals (CLLCs) infiltrated throughout with high densities of noble metals. We present a detailed study of the optical response of individual CLLCs in order to reveal further information on the structure and alignment of the metal inclusions and their associated plasmonic response. In general, we expect a qualitatively different optical response depending on the morphology of the nanometallic inclusions and their 3D arrangement within the solvent channels of the cross-linked protein crystal. In particular, any form of connectivity between the nanometallic structures located in the solvent channels should be evidenced optically by a complex metamaterial response, including near-zero permittivity and negative index behavior.[12,13] More broadly, the precise structural arrangement of the hybrid organic-inorganic nanostructures is of considerable importance for applications involving the chemical and optical characteristics of these materials.

Dr. O. L. Muskens
Physics and Astonomy
Faculty of Physical and Applied Sciences
University of Southampton
Highfield, Southampton SO17 1BJ, UK
E-mail: o.muskens@soton.ac.uk
M. W. England, Dr. M. Li, Prof. S. Mann
Centre for Organized Matter Chemistry
School of Chemistry
University of Bristol
BS8 1TS, UK; E-mail: s.mann@bristol.ac.uk
Dr. L. Danos
Faculty of Engineering
University of Southampton
Highfield, Southampton SO17 1BJ, UK

DOI: 10.1002/adfm.201201718

2. Results and Discussion

2.1. Angle-Dependent Reflection and Transmission Measurements

Scheme 1 shows the experimental configuration used for reflection and transmission optical measurements of as-prepared

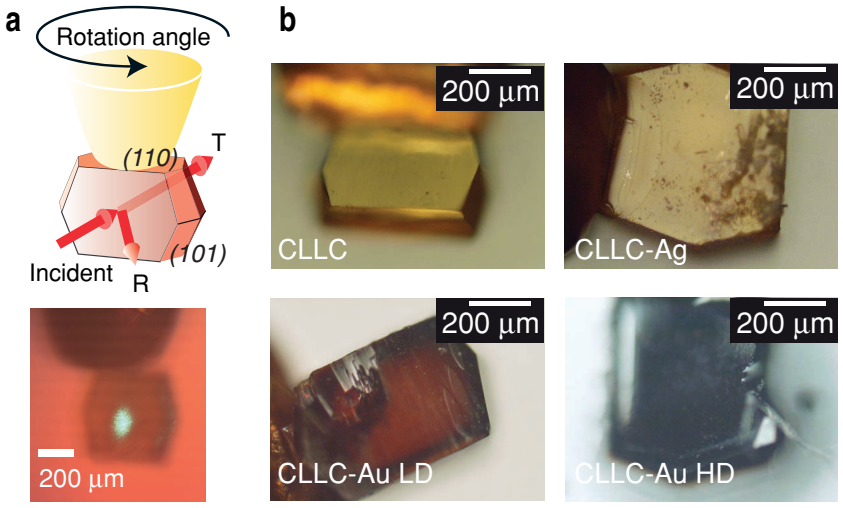

Scheme 1. a) Experimental configuration for reflection and transmission measurements on single lysozyme crystals (top left panel) and corresponding image (bottom left panel) of crystal and laser beam in the optical setup. b) Optical microscopy images showing a CLLC before metal infiltration, a Ag-filled CLLC (CLLC-Ag), and a Au-filled CLLCs of low- or high-density (CLLC-Au LD/HD).

or metal-infiltrated single CLLCs (see Experimental Section for details on synthesis and infiltration procedure), and typical optical microscopy images of the hybrid materials. As described elsewhere,[8] the metal-infiltrated CLLCs were well-ordered single crystals. While the pure CLLCs showed a yellow transparent transmission, crystals filled with Au were dark red to black with increasing Au infiltration. Gravimetric analysis revealed that Au samples contained 23 wt% of Au for the samples made using one infiltration cycle (low-density or CLLC-Au LD) and 36 wt% for the samples made using two cycles (high-density or CLLC-Au HD). In contrast, the Ag-filled CLLCs, containing 10 wt% of Ag, were brown in colour. These visual characteristics were indicative of a strong effect of the metal inclusions on the optical response as demonstrated in the optical transmission and reflection measurements on individual crystals (**Figure 1**). To investigate effects of anisotropy, measurements were taken for two polarizations and for three angles of incidence of 10°, 30° and 50°. Individual pure CLLCs showed high transmission in the visible, and a broad absorption band in the near-infrared (Figure 1a). UV-vis spectra of solutions of lysozyme and the glutaraldehyde cross-linker showed no infrared absorption peaks in this spectral region (Figure S1, Supporting Information), therefore the infrared absorption band was attributed to residual water incorporated in the crystal. No significant dependence on polarization was found for the pure CLLCs, in agreement with the low intrinsic birefringence of around 3×10^{-3} reported earlier for lysozyme crystals.[14] In contrast, transmission spectra of Ag- or Au-infiltrated CLLCs showed additional absorption bands in the range 400–550 nm (Figure 1b,c). These absorption bands were consistent with the localized surface plasmon resonance (LSPR) of isotropic Ag and Au nanoclusters.[15,16] However, a much broader absorption band extending over the entire spectral range under study characterized the low transmission observed for Au-infiltrated CLLCs prepared at high-density metallic loadings (Figure 1d). This was indicative of a more complex internal

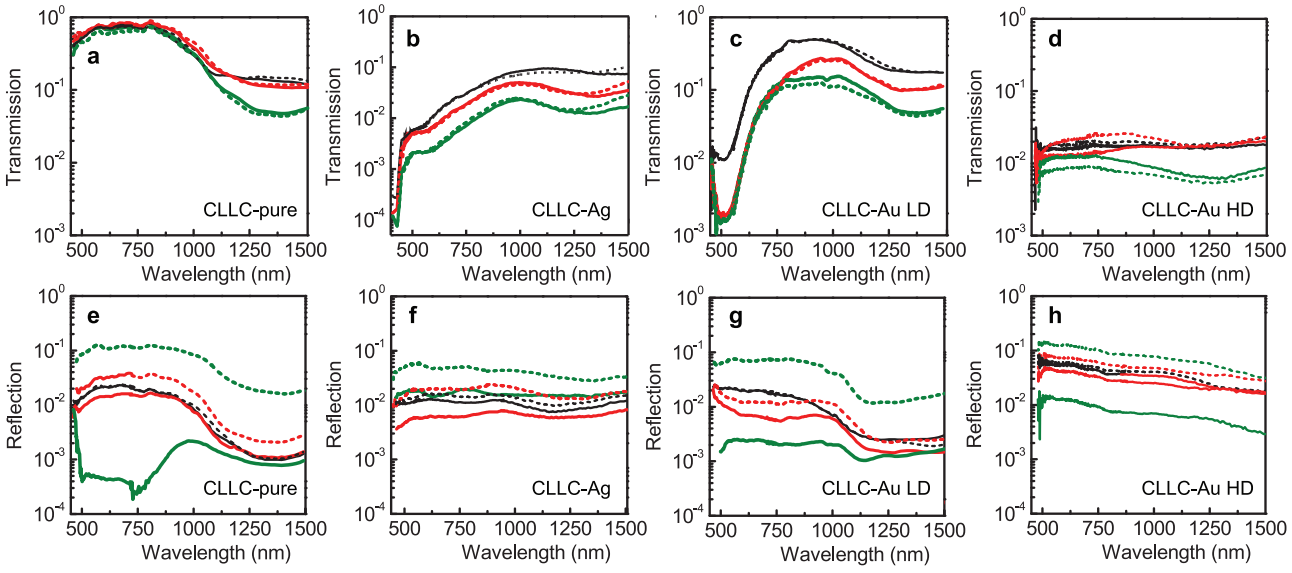

Figure 1. Angle- and polarization-resolved transmission (a–d) and reflection (e–h) spectra from single CLLCs before or after metal infiltration. a,e) as-prepared CLLC without metal infiltration, b,f), Ag-infiltrated CLLC, c,g) low density (LD) loaded Au-infiltrated CLLC, and d,h) high density (HD) loaded Au-CLLC. Colors indicate angles of incidence of 10° (black), 30° (red), and 50° (green). Solid curves correspond to transverse magnetic (TM) polarization, dashed curves correspond to transverse electric (TE) polarization.

structure for the intracrystalline Au inclusions, which could not be readily explained by a simple spherical particle model. None of the crystals under study showed a pronounced dependence of the resonant absorption band on the polarization of the incident light, and no dependence on angle of incidence was observed, apart from an overall decrease that was consistent with the increased path length through the crystal. For the Ag-filled CLLCs, a pronounced effect of ageing was observed over a time scale of several days, characterized by a suppression of the resonant absorption band and the appearance of a broad absorption covering the entire visible and infrared range. This change was consistent with the oxidation of Ag and concomitant loss of the plasmonic response.

The absence of resonant plasmonic features in the reflection spectra (see Figure 1f–h) indicated that the absorption originated from nanoclusters located deep inside the crystal, rather than from surface contamination. Increasing the angle resulted in a decrease in the reflectivity of TM (horizontal) polarization and an increase for TE (vertical) polarization for all the samples, consistent with Fresnel reflections from the lysozyme host material with an expected Brewster's angle at around 50° for the low-index organic crystal.

2.2. Interpretation of Absorption Spectra Using a Spheroidal Model

Given the above observations, we analysed the optical response of the metal-filled CLLCs using a spheroidal cluster model. Following the Lambert-Beer law, the absorption coefficient is given by $\mu = \eta\sigma_a/V_p$, where η is the volume fraction of nanoparticles, V_p the particle volume, and σ_a the particle absorption cross section. According to Equation (1) (see Experimental Section), μ is in approximation independent of particle size and is given, for a spherical particle, by $\mu \approx (1.8 \times 10^{-8})\eta$ at the LSPR wavelength of 520 nm (for a more detailed treatment, see ref. [15–19]. **Figure 2**a–c shows optical absorption coefficients for a number of metal-infiltrated CLLCs obtained from the transmission spectra at 0° angle of incidence. Results for pure CLLC are shown in Figure S2 (Supporting Information). A typical value for μ for a Au-infiltrated CLLC was 2.5×10^4 m^{-1} (Figure 2b), which corresponded to a volume fraction of Au of $\eta = 4.6 \times 10^{-4}$. Given the large ratio of the mass densities of 1.21 g cm^{-3} for a pure lysozyme crystal[20] and 19.3 g cm^{-3} for Au, the conversion between vol% and wt% is a factor 16. The weight percentage obtained using the value for μ from the peak absorption only thus resulted in a value one order of magnitude less than that from the gravimetric measurements on crystals.[8] This apparent discrepancy can be explained partly by inhomogeneous broadening of the LSPR absorption band over a wide spectral region extending into the near-infrared region, as is observed in Figure 2a–c. Such a broadening may be caused by a distribution of elongated gold nanoclusters, where an increase of the particle aspect ratio results in a redshift of the LSPR corresponding to the long particle axis.[21] Alternatively, a redshift is also observed for spherical particles that are closely spaced and strongly interacting.[22] For such a coupling to produce the amount of experimentally observed LSPR lineshift, the nanoparticles have to be spaced within less than 1.2 times their diameter.[23,24] Significant shifts of the LSPR have been observed in nanoparticle effective media only for volume fractions of Au larger than 10 vol%.[25] Based on the gravimetric estimate of 36 wt%, the largest volume fraction achieved in the Au-HD crystals was 2.25 vol%; this corresponds to an average nanoparticle spacing of around 3.5 times their diameter (calculated from the inverse cube root of the volume fraction, an assumption valid for the large pore densities of lysozyme crystals). For a completely homogeneous distribution of spherical particles this rules out particle-particle interaction as the source for inhomogeneous broadening of the LSPR absorption band.

The mass density of Au-clusters produced by the sequestration method[8] is significantly higher than those obtained in recent studies using other methods.[6,7] However, the large variation in both spectral width and amplitude of the LSPR absorption between different crystals of each type of metal-filled CLLC indicates that despite being produced at the same time using exactly the same procedure, not all crystals contain the same amount of metal infiltration or material distribution. In part, this may be due to the reaction procedure, which relies critically on the rates at which the intercalated sodium borohydride diffuses out and Au(III) complex diffuses into the crystals. Controlling these rates is difficult, so changes in local concentration or differences in time of soaking the crystals could make a significant difference. These results call for more systematic studies, for example, through in-situ growth monitoring or comparison of crystals with different sizes and morphologies, to address these issues.

We modelled the degree of heterogeneous broadening in the Au-CLLCs using Equation (1) (see Experimental Section), assuming a distribution of spheroidal particles with aspect ratios ranging from 1 to 11. The absorption spectra were fitted using a nonlinear least-squares method over the range 450–1200 nm. Good agreement was obtained for the general shape of the absorption profiles for all samples under study (see dashed lines in Figure 2a–c). A small ripple on the fitted curves was due to the discrete number of aspect ratios in the fit. The fits yielded distributions of the volume fraction versus the aspect ratio (a/b) of the Au clusters (Figure 2d–f). By summing up the relative volume fractions for all aspect ratios, a total volume fraction, η_{tot}, was obtained for each sample, and plotted parametrically against the average aspect ratio in **Figure 3**. The data points for the different types of Ag- and Au-infiltrated crystals were clearly clustered, and the average aspect ratio reached values as high as 4.0 for the high-density Au-CLLCs. Given a solvent channel diameter of 2.5 nm, these results indicated the presence of individual metallic segments of up to 10 nm in length. Moreover, given the relatively low volume fraction (ca. 2.25 vol% at an Au loading of 36 wt% assuming bulk densities), the observed broad optical response is consistent with a heterogeneous distribution in the location of the Au nanoclusters throughout the protein matrix. Indeed, the approximately Gaussian distribution of aspect ratios in Figure 2d–f was consistent with a statistical variation resulting from random processes within the confined spaces of the solvent channels.

The above optical data indicate that the nucleation mechanism favours formation of a mixture of isolated or weakly coupled clusters with spheroidal or anisotropic form, and that there appears to be no energetic advantage for the formation of

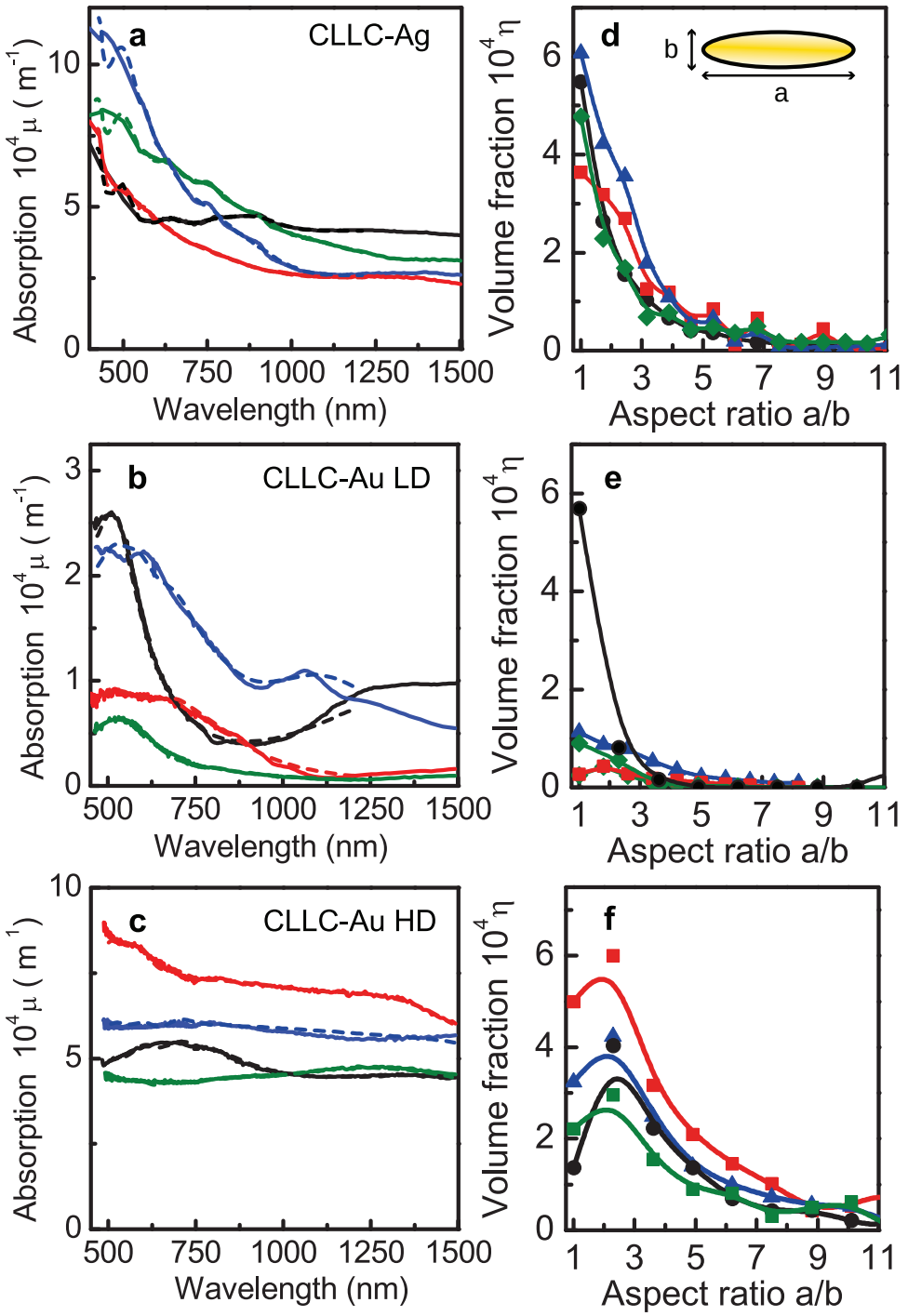

Figure 2. a–c) Absorption coefficients, μ, obtained from transmission spectra from metal-filled CLLCs. d–f) Nanoparticle aspect ratio distributions obtained from fits of the absorption spectra. Absorption spectra for pure CLLCs, see Supporting Information (Figure S2). Different colors represent different single crystals in each sample.

extended nanowires within the solvent channels of the CLLCs. Moreover, as no dependence on both polarization and angle of incidence was observed, macroscopic alignment of the anisotropic nanoclusters seems highly unlikely. This is surprising since nucleation of the metallic nanoclusters takes place within the periodically aligned solvent channels. However, the solvent channels permeating the tetragonal structure of lysozyme are irregular in shape and helicity,[5] and it may be that these topographical heterogeneities facilitate a wide variety of particle morphologies and orientations within the intracrystalline

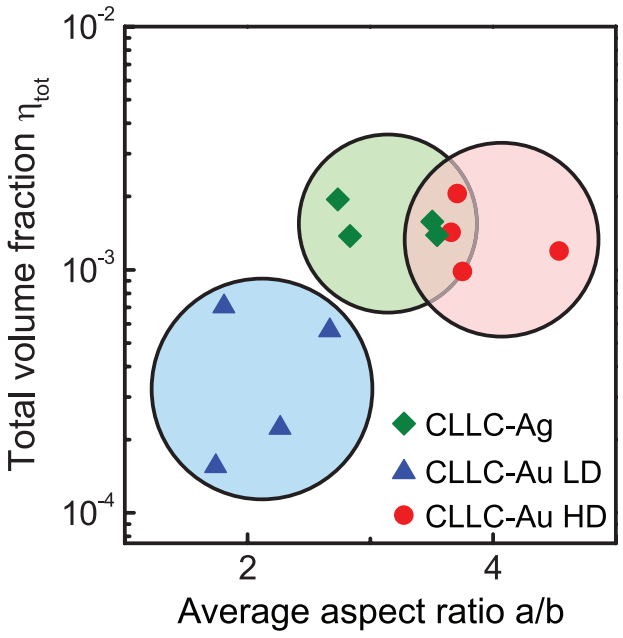

Figure 3. Parametric plot of the fitted total volume fraction against average aspect ratio for as-prepared and metal-infiltrated CLLCs. In each case, circles indicate approximate distribution radius for the different samples.

protein matrix. Alternatively, it is possible that the crystalline porous structure is disrupted locally by the chemical treatments involved in cross-linking and sequestration; however, single crystal X-ray diffraction studies indicated a globally intact crystal structure.[8] Despite the lack of macroscopic alignment, the optical measurements support the general model of a percolating network of nanopores containing a significant amount of metal nanoclusters, some of which exhibit moderate anisotropy.

2.3. Birefringence of Au-Infiltrated CLLCs

Lysozyme crystals have been reported to have an intrinsic form-birefringence of around 10^{-3} due to the crystalline nanostructure and presence of aligned solvent channels along the [001] (c-)axis.[14] We therefore used polarization interferometry as a sensitive probe of the internal structure of the crystals before and after Au-infiltration. Specifically, we determined the polarization contrast (C_{pol}, see Experimental Section), which varied between –1.0 and 1.0, indicating linear polarization states perpendicular and parallel to the input polarization, respectively. **Figure 4**a,b shows the transmission and polarization contrast obtained for three representative crystals, an as-prepared pure CLLC, and Au-filled CLLCs of low and high density. Here, the

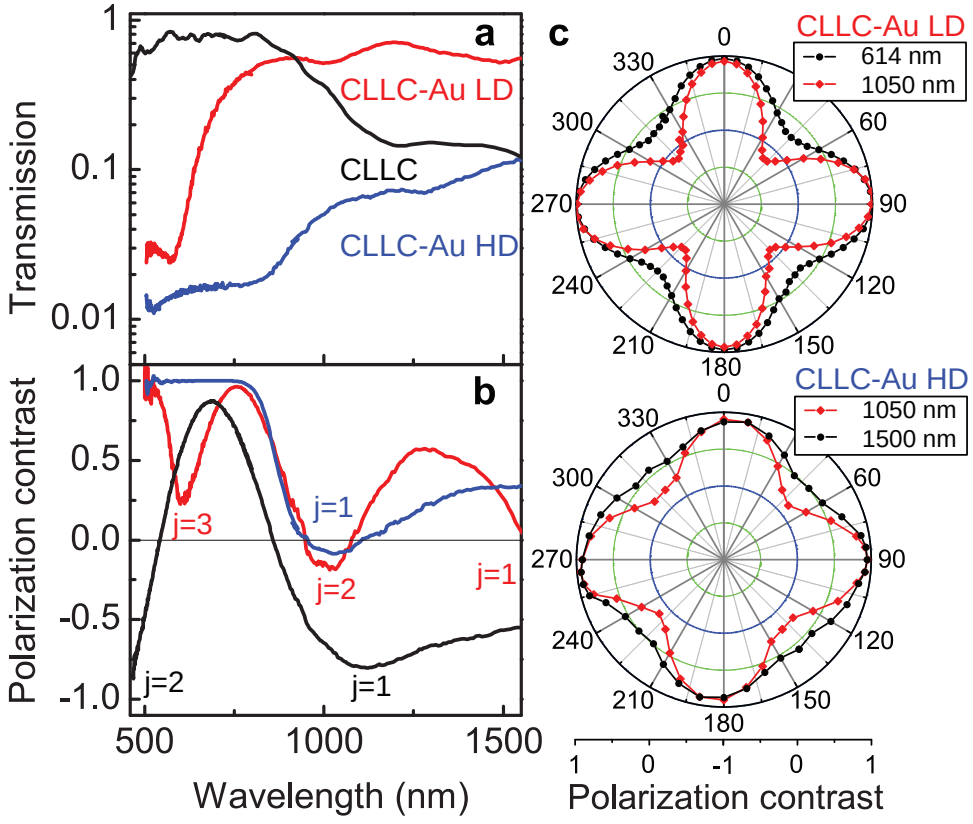

Figure 4. a) Optical transmission and b) polarization interferometry contrast of a pure CLLC (black, 180 µm thickness), a Au-filled CLLC with low density (red, 380 µm thickness) and a Au-filled CLLC with high-density (blue, 130 µm thickness), for incident polarization of 45°. c) Dependence of polarization contrast on the angle between the crystallographic c-axis and the incident polarization vector for the Au-filled CLLCs at two characteristic wavelengths.

angle between the input polarization and the crystal axis was fixed at 45° for maximal polarization conversion. We observed clear oscillations in the polarization contrast for all three samples (note the large difference in sample thickness resulting in different oscillation periods). The pure CLLC showed a high transmission and a large contrast between polarization states. The rotation of the polarization state can be described by the relative retardance of the optical waves along the slow and fast crystal axes; that is $\delta = 2\pi\Delta nL/\lambda$ where Δn is the birefringence, L is the path length and λ is the wavelength. When the retardance equals π, 3π… a minimum in the contrast is obtained, which results in a value for the birefringence, $\Delta n = (2j-1)\lambda/2L$, where j denotes the order of the retardance. For the pure CLLC, we obtained a value of $\Delta n = 3.1 \times 10^{-3}$, comparable to the value for pure non-cross-linked lysozyme. For the Au-infiltrated crystals, we observed a similar oscillation in the polarization contrast at long wavelengths, where the influence of the LSPR absorption was small. This shows that the crystallographic anisotropy is conserved after infiltration of metals in the protein solvent channels. In the wavelength range where the LSPR absorption is strong, the oscillation in the contrast becomes less pronounced in the low-density CLLC-Au LD sample, and completely disappears in the high-density CLLC-Au HD sample.

We further investigated the polarization conversion process by measuring the contrast as a function of angle between the incident polarization and the crystal axis, as is shown in the polar plots of Figure 4c. At an angle of 0°, the polarization direction is aligned with the crystal axis and no birefringence occurs, while at an angle of 45° the polarization rotation is largest, resulting in a minimum contrast. At all wavelengths under study, the contrast at 0° approached 1.0, signifying that a beam of linear polarized light was transmitted through the sample and thus that the contribution of unpolarized scattering was low.

A possible explanation of the behaviour of the polarisation contrast for the metal-infiltrated crystals is that the birefringence is modified in the LSPR wavelength region by the presence of metal inclusions. The LSPR absorption is associated with a real part of the refractive index, as can be calculated from effective medium models. The filling up of solvent channels with metals results in a replacement of the refractive index of air by that of the gold nanoclusters. The refractive contrast between solvent channels and protein, which plays a role in the form-birefringence, is therefore reduced, more strongly around the LSPR. At wavelengths far removed from the plasmon resonance, the effect of the nanoparticles is smaller and the original birefringence is recovered. Indeed, we find values of Δn of 4.1×10^{-3} and 3.8×10^{-3} for the low and high Au densities, respectively, using the minimum in polarization contrast at near infrared wavelengths.

2.4. Fluorescence Emission of Au-Infiltrated CLLCs

Recently, protein-protected gold clusters have received considerable attention for their use as fluorescent labels.[26–29] We investigated the fluorescence emission of Au-filled CLLCs using both fluorescence spectroscopy and lifetime measurements. **Figure 5** shows fluorescence emission spectra of pure

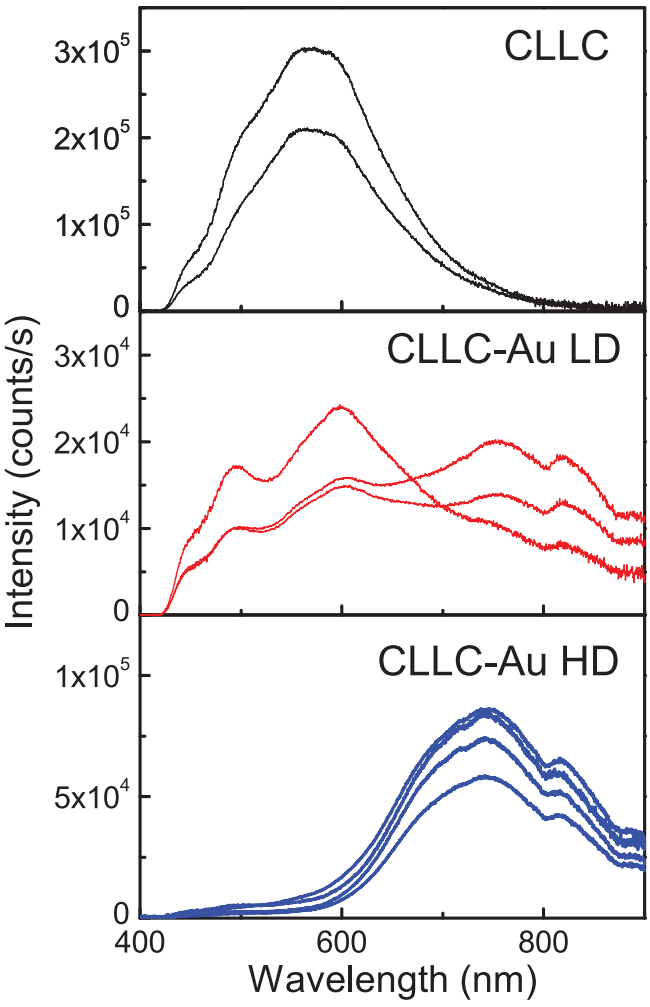

Figure 5. Fluorescence spectra for 405 nm excitation for a) CLLC, b) CLLC-Au LD, and c) CLLC-Au HD. Curves represent different individual crystals.

CLLCs and of Au-infiltrated CLLCs at low and at high Au densities. The pure CLLCs, without any Au-inclusions, show a bright white emission which is spectrally peaked around 570 nm. Similar emission spectra have been reported in several recent studies and have been attributed to the emission from delocalized electrons engaged in hydrogen bonding.[30–33] The emission is generic for different types of proteins and occurs both in solutions and single-crystals of proteins. The Au-filled crystals show a significantly weaker fluorescence emission, which is shifted toward longer wavelengths.

The fluorescence emission from Au-infiltrated CLLCs may be explained by two independent contributions. Firstly, the emission from the protein host crystal may be modified by quenching at the LSPR wavelength and by reabsorption of emitted photons by the nanoparticles. Secondly, there may be an emission from Au clusters or larger nanoparticles embedded inside the matrix. Emission of small Au clusters strongly depends on the size of the particles and can range from <500 nm for Au_8 to >800 nm for Au_{28}.[26–29] For particles of larger size, the emission is determined by the interband transitions of the bulk material,

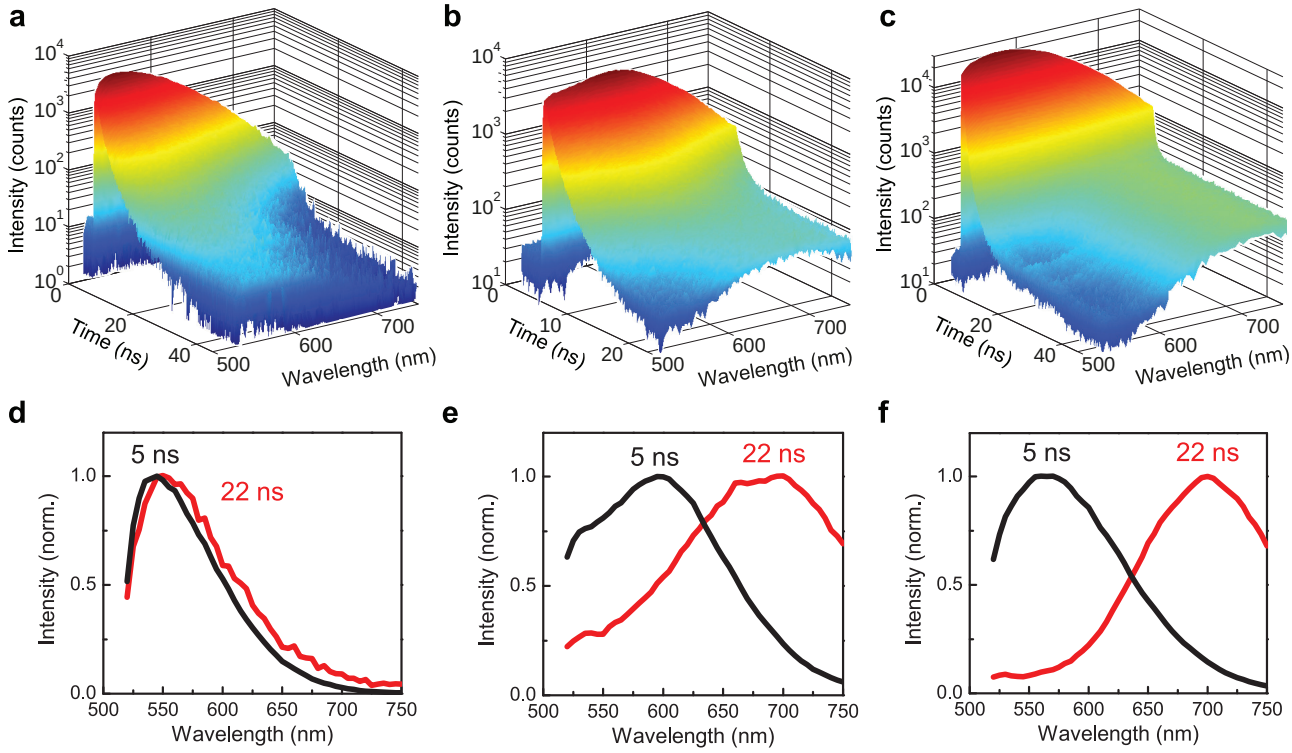

Figure 6. Time-resolved fluorescence decay spectra (log-scale) of a) pure CLLC, b) CLLC-Au LD, and c) CLLC-Au HD. d–f) Normalized spectra of fast component taken at 0.5 ns delay and stationary component taken at 22 ns delay. Fast component corresponds to pure CLLC emission, slow component is assigned to Au nanocluster fluorescence.

modified by the local field factor at the emission wavelength resulting from the LSPR.[34–36] To separate these various contributions we have performed fluorescence lifetime spectroscopy on representative crystals. **Figure 6**a–c shows spectrally resolved lifetime decays of the three types of CLLC. The lifetime images allow identification of a component with decay time of the order of ns, and a slow component which forms a constant background on the time scale of our experiment which is present only for the two CLLC-Au samples. The spectral signatures of both components is illustrated in Figure 6d–f, which show the normalized spectra at the maximum of the decay curve and at the stationary level around 22 ns. The fast, nanosecond component corresponds to the fluorescence of the protein host crystal. The fluorescence decay of this fast component, after subtraction of the slow background, is shown in **Figure 7** and could be fitted to good accuracy see Figure S3–S5, Supporting Information) using a tri-exponential decay with time constants of 0.65 ns, 1.95 ns and 6.83 ns, and respective relative amplitudes of 45.8%, 46.2% and 8%. A similar tri-exponential decay was observed in protein solutions.[31] An average decay time can be defined from the weighted average of the three exponentials, resulting in a value of 3.43 ns for the pure CLLC. The fluorescence decay time shows an decrease with increasing Au content, with respective values of 2.18 ns and 1.05 ns for the CLLC-Au of low-density and high-density (for full tri-exponential decay fits see Table S1, Supporting Information). Combined with the strong reduction of the overall emission intensity from the Au-filled crystals, we interpreted the reduction of the decay rate as a quenching of the protein fluorescence due to nonradiative coupling to the SPR of the Au clusters.

In contrast to the fast component, which is observed for all crystals under study, the slow component in Figure 6 is only

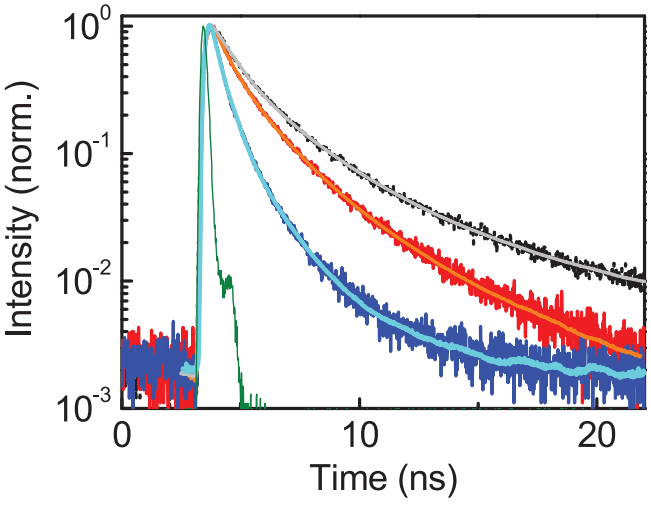

Figure 7. Time-resolved fluorescence decay curves at 580 nm wavelength, after subtraction of background intensity, for pure CLLC (black), CLLC-Au LD (red), and CLLC-Au HD (blue), with triexponential fits including instrument response, resulting in amplitude-weighted average decay times of 3.43 ns, 2.18 ns, and 1.05 ns (chi-squared <1.25), respectively. Green line: instrument response function.

present for the Au-filled CLLCs and is attributed to emission from Au nanoclusters. Emission in small Au clusters has been attributed as originating from the singlet- and triplet-states of the molecular-type cluster and has a long emission in the microsecond range.[28] This long-time decay could not be measured here due to prohibitively low count rates at the required repetition frequencies of the excitation laser. In contrast, it is well known that emission from larger nanoparticles originates from electron-hole recombination on a time-scale <50 fs,[34] which is not observed in our experiment. Thus, we attribute the emission band at 700 nm to emission from small Au clusters embedded in the lysozyme host material. No evidence was found in the decay spectra for energy transfer from lysozyme excitations to the SPR contributing to the nanocluster emission; all spectral decay curves could be fitted with high accuracy ($\chi^2 < 1.3$) using a global set of decay times for each sample over the entire spectrum (see Figure S6, Supporting Information). This indicates the absence of a variation in decay channels over the spectral range.

3. Conclusions

In conclusion, we have performed a detailed investigation of the optical response of lysozyme single crystals infiltrated with Ag and Au nanophases. We have demonstrated the presence of a plasmonic response in both types of metal-filled crystals, and have assigned this response to the surface plasmon resonance of isolated gold nanoclusters with spheroidal or moderately anisotropic morphology, and which are specifically located within the periodically arranged solvent channels of the protein matrix. No evidence for continuous nanowires was obtained. Birefringence measurements confirmed that both pure and infiltrated CLLCs show an equal birefringence in the near-infrared, where the effect of plasmon resonance is relatively weak. In contrast, no birefringence was observed on the plasmon absorption peak, indicating an effect of the nanoparticle dielectric response on the effective refractive index. Fluorescence decay spectroscopy revealed contributions attributed to fluorescence from the protein crystal, with in addition a slow contribution which is consistent with the emission from the molecular-like states of small Au nanoclusters. We emphasize that the signatures of spheroidical particles in the transmission and small Au nanoclusters in the fluorescence are not in mutual contradiction. Most likely, a wide distribution of metal inclusions are present inside the protein host; different types of nanoclusters contribute to different aspects of the optical response. The emission peak around 650–750 nm wavelength is consistent with the fluorescence of <1 nm clusters (typically Au_{25}), and is consistent with previous observations in Au-protein complexes.[10,26] However, the LSPR absorption of such small clusters is strongly suppressed compared to the semiclassical Drude model, due to the quantization of energy levels and the increasing role of electron-surface scattering which damp the collective electronic oscillation. For larger-sized nanoparticles >1 nm, LSPR absorption is predominant, but fluorescence emission is strongly reduced due to the short, femtosecond lifetime of the photoexcited carriers.[34] The presence of a large fraction of small nanoclusters, exhibiting a strongly suppressed resonant LSPR absorption may also explain the discrepancies between gravimetric and optical-based estimates of the metal fraction.

Our data indicate an absence of coherent alignment of the Au inclusions within the interior of the CLLCs, but more studies are needed to address the nanoscopic morphology of these new metamaterials in more detail. The absence of interconnectivity between the nanoclusters in the solvent channels suggests that the protein crystals might not exhibit ohmic electrical conductivity, although we cannot rule out the possibility of intra-crystalline electron transport via non-classical quantum tunnelling mechanisms. On the other hand, the large specific area, confined organization, and isolated morphology could be beneficial for applications in catalysis,[37] and may be of considerable interest for biological applications involving the surface plasmon resonance behaviour of the protein-entrapped spherical gold nanoclusters.

4. Experimental Section

Synthesis of Cross-Linked Lysozyme Crystals: For the preparation of lysozyme crystals, a liquid/liquid interface method was used to minimize mechanical damage, and maximize crystal size.[38] A crystallization solution (10 mL) of NaCl (60 mg mL^{-1}) and NaOAc buffer (8.2 mg mL^{-1}) was made up at pH 4. Hen egg white lysozyme (20 mg mL^{-1}) was then dissolved in the solution, with rapid stirring. The solution was then filtered into a glass vial containing dichloromethane (3–5 mL), and left for up to 48 h. The crystallization solution and dichloromethane were removed, and a cross-linking solution (10 mL, 8.2 mg mL^{-1} NaOAc, 60 mg mL^{-1} NaCl, pH 4) containing glutaraldehyde (1–5%) was added. The crystals were left for a 24–48 h, and were then washed with water and dried under vacuum for 1–3 h. Au infiltrated crystals were prepared by soaking CLLCs in $NaBH_4$ (10^{-5} M) for 10 min, washed with water, and dried under vacuum for 1–3 h. The borohydride-containing crystals were then soaked in $HAuCl_4 \cdot 3H_2O$ (10^{-5} M) for 3 days, washed with water, and dried under vacuum for 1–3 h. Concentrated Au crystals were prepared by repeating the steps described for the original Au deposition, using a crystal that had previously undergone the Au deposition process. Ag infiltrated crystals were prepared be soaking CLLCs in $AgNO_3$ (10^{-3}–10^{-5} M) for 3 days, in the dark, then exposing them to UV-radiation (wavelength 254 nm) for 6 h. Extensive structural investigation of metal-loaded CLLCs including HRTEM and single-crystal X-ray diffraction have been reported in ref. [8,9]. The cross-linked crystals showed no significant change in crystallographic structure.

Optical Experiments: Individual crystals were fixed using different methods. Larger crystals were glued to the tip of a copper wire and positioned with the prismatic facets perpendicular to the plane of rotation, as shown in Scheme 1a. Crystals with dimensions smaller than 200 μm were fixed to a glass slide using PMMA, where the optical access was kept clear. Transmission and reflection measurements were taken using a sensitive wavelength-scanning UV-vis setup based on lock-in detection. The angle was varied using a motorized rotation stage, while linear polarizations of the incident light were selected using a polarizer. Transmitted and reflected intensities were collected over an approximately 2° wide angular cone by using an integrating sphere equipped with Si and InGaAs detectors, covering the range 450–1800 nm. Polarization interferometry measurements were done following the method of ref. [39] In short, two polarizers were mounted in the incident and transmitted light paths at polarization angles of 45° with respect to the crystallographic c-axis. The polarization contrast C_{pol} was measured between parallel- polarized ($I_{\parallel}$) and cross-polarized ($I_{\perp}$) configurations using the relation

$$C_{pol} = \frac{I_{\parallel} - I_{\perp}}{I_{\parallel} + I_{\perp}}$$

Interpretation of Absorption Spectra Using a Spheroidal Model: Using the experimental absorption data, the concentration of gold nanoparticles was estimated using the known absorbance of a small gold spheroid. For small particles of a few nanometer diameter, the LSPR absorption cross-section is proportional to the particle volume, and given by Rayleigh-Gans theory for a spheroid according to[15,16]

$$\sigma_a = \frac{2\pi V_p \varepsilon_m^{3/2}}{\lambda L_i^2} \frac{\varepsilon(\lambda)}{|\varepsilon(\lambda) + \varepsilon_m (1 - L_i)/L_i|^2} \quad (1)$$

Here, $\varepsilon(\lambda)$ is the wavelength-dependent dielectric function of the metal, with $\varepsilon''(\lambda)$ its imaginary part; ε_m denotes the dielectric constant of the surrounding material, for the nanoporous lysozyme material $\varepsilon_m \approx 1.5$. The parameters L_i are the depolarization factors along the principal axes, which for a prolate geometry are given by[15]

$$L_1 = \frac{1 - e^2}{e^2}\left[\frac{1}{2e}\ln\left(\frac{1+e}{1-e}\right) - 1\right], \; L_{2,3} = (1 - L_1)/2 \quad (2)$$

Here e is the eccentricity defined as $e = (1 - b^2/a^2)^{1/2}$ with a/b the aspect ratio of the spheroid, and for a sphere, $L_{1,2,3} = 1/3$. For the dielectric function of the metal, we used the experimental values for bulk Au[18] and Ag[19] modified by a correction for surface scattering in the small nanoparticles given by[15,16]

$$\varepsilon = \varepsilon^{bulk} + \frac{\omega_p^2}{\omega(\omega + i\gamma_{bulk})} - \frac{\omega_p^2}{\omega(\omega + i\gamma)} \quad (3)$$

where γ_{bulk} and γ are the bulk and nanoparticle Drude damping rates. The nanoparticle damping rate γ is given by

$$\gamma = \gamma_{bulk} + 2g\upsilon_F/D \quad (4)$$

where ν_F denotes the Fermi velocity and g is a factor representing the surface damping strength which is commonly assumed of order 1. In our model, we assumed a diameter of 2.5 nm, as given by the pore size. We tried different values of D but found that this had only a small effect on the data fitting.

Fluorescence Spectroscopy: Fluorescence emission spectra were collected using illumination by a CW diode laser at 405 nm at an optical power of 3 mW. Fluorescence emission was collected by a lens with numerical aperture of 0.5 and detected using a fibre spectrometer using integration times between 0.1 s and 2 s (Ocean Optics). Spectra were corrected for the spectral response of the spectrometer against known standards (correction factor was scaled to 1.0 at a wavelength of 550 nm).[40] Fluorescence lifetime measurements were taken employing a time-correlated photon counting[41] setup (FluoTime200, Picoquant) using a 475-nm picosecond pulsed diode laser (PicoQuant, LDH485) at an average optical power of 0.5 mW and with a variable repletion rate (20–40 MHz). Detected light was spectrally selected using a monochromator (Scientech 9030) and detected using a photomultiplier. The instrument's response function (IRF) had a full-width at half-maximum of 200 ps.

Analysis: The fluorescence decay curves were analysed using the FLUOFIT software (PicoQuant, version 4.2.1) based on tri-exponential model which involves an iterative reconvolution process.[42] The quality of the fit was assessed by the value of the reduced χ^2 value (a value of less than 1.30 for an acceptable fit), and from a visual inspection of the distribution of the weighted residuals and their autocorrelation function.[43]

The time-resolved emission spectra (TRES) were recorded at different wavelengths, in this case 520–750 nm with a 5 nm step

Supporting Information

Supporting Information is available from the Wiley Online Library or from the author.

Acknowledgements

The authors thank EPSRC, Unilever Research, and ERC for financial support, E. Lambert for fruitful discussions, and S. Hyett for assistance with optical experiments.

Received: June 24, 2012
Published online: August 15, 2012

[1] H. Furukawa, N. Ko, Y. B. Go, N. Aratani, S. B. Choi, E. Choi, A. O. Yazaydin, R. Q. Snurr, M. O'Keeffe, J. Kim, O. M. Yaghi, *Science* **2010**, *329*, 424.
[2] A. Horike S. Shimomura, S. Kitagawa, *Nat. Chem.* **2009**, *1*, 695.
[3] J. Rabone, Y.-F. Yue, S. Y. Chong, K. C. Stylianou, J. Bacsa, D. Bradshaw, G. R. Darling, N. G. Berry, Y. Z. Khimyak, A. Y. Ganin, P. Wiper, J. B. Claridge, M. J. Rosseinsky, *Science* **2010**, *329*, 1053.
[4] K. Chaudhari, P. Lourdu Xavier, T. Pradeep, *ACS Nano* **2011**, *5*, 8816.
[5] J. C. Falkner, A. M. Al-Somali, J. J. Jamison, J. Zhang, S. L. Adrianse, R. L. Simpson, M. K. Calabretta, W. Radding, G. N. Phillips, V. L. Colvin, *Chem. Mater.* **2005**, *17*, 2679.
[6] S. Das, A. Kumar Sahoo, S. Sankar Ghosh, A. Chattopadhyay, *Langmuir* **2010**, *26*, 15714.
[7] H. Wei, Z. Wang, J. Zhang, S. House, Y.-G. Gao, L. Yang, H. Robinson, L. H. Tan, H. Xing, C. Hou, I. M. Robertson, J.-M. Zuo, Y. Lu, *Nat. Nanotechnol.* **2011**, *6*, 93.
[8] M. Guli, E. M. Lambert, M. Li, S. Mann, *Angew. Chem. Int. Ed.* **2010**, *49*, 520.
[9] E. M. Lambert, *Organization of protein biomolecules for the template-assisted preparation of higher-order inorganic materials*, PhD Thesis, University of Bristol, **2010**.
[10] C. L. Liu, H. T. Wu, Y. H. Hsiao, C. W. Lai, C. W. Shih, Y.-K. Peng, K.-C. Tang, H.-W. Chang, Y.-C. Chien, J.-K. Hsiao, J.-T. Cheng, P.-T. Chou, *Angew. Chem. Int. Ed.* **2011**, *50*, 7056.
[11] H. Wei, Y. Lu, *Chem. Asian J.* **2012**, *7*, 680.
[12] R. J. Pollard, A. Murphy, W. R. Hendren, P. R. Evans, R. Atkinson, G. A. Wurtz, and A. V. Zayats, V. A. Podolskiy, *Phys. Rev. Lett.* **2009**, *102*, 127405.
[13] J. Yao, Z. Liu, Y. Liu, Y. Wang, C. Sun, G. Bartal, A. M. Stacy, X. Zhang, *Science* **2008**, *321*, 930.
[14] W. Singer, H. Rubinsztein-Dunlop, U. Gibson, *Opt. Express* **2004**, *12*, 6440.
[15] U. Kreibig, M. Vollmer *Optical Properties of Metal Clusters*, Springer, Berlin **1995**.
[16] O. L. Muskens, P. Billaud, M. Broyer, N. Del Fatti, F. Vallée, *Phys. Rev. B* **2008**, *78*, 205410.
[17] W. Haiss, N. T. K. Thanh, J. Aveyard, D. G. Fernig, *Anal. Chem.* **2007**, *79*, 4215.
[18] P. B. Johnson, R. W. Christie, *Phys. Rev. B* **1972**, *6*, 4370.
[19] E. D. Palik, *Handbook of Optical Constants of Solids*, Academic Press, New York **1985**.
[20] M. Tachibana, K. Kojima, R. Ikuyama, Y. Kobayashi, M. Ataka, *Chem. Phys. Lett.* **2000**, *332*, 259.
[21] S. Link, M. A. El-Sayed, *J. Phys. Chem. B* **1999**, *103*, 8410.
[22] S. Lin, M. Li, E. Dujardin, C. Girard, S. Mann, *Adv. Mater.* **2005**, *17*, 2553.
[23] K.-H. Su, Q.-H. Wei, and X. Zhang, J. J. Mock, D. R. Smith, S. Schultz, *Nano Lett.* **2003**, *3*, 1087.
[24] Y.-L Chiang, C.-W. Chen, C.-H. Wang, C.-Y. Hsieh, Y.-T. Chen, H.-Y. Shih, Y.-F. Chen, *Appl. Phys. Lett.* **2010**, *96*, 041904.
[25] T. Ung, L. M. Liz-Marzán, P. Mulvaney, *J. Phys. Chem. B* **2001**, *105*, 3441.
[26] P. L. Xavier, K. Chaudhari, A. Baksi, P. Thalappil, *Nano Rev.* **2012**, *3*, 14767.

[27] M. B. Mohamed, V. Volkov, S. Link, M. A. El-Sayed, *Chem. Phys. Lett.* **2000**, *317*, 517.
[28] S. Link, A. Beeby, S. FitzGerald, M. A. El-Sayed, T. G. Schaaff, R. L. Whetten, *J. Phys. Chem. B* **2002**, *106*, 3410.
[29] J. Zheng, J. T. Petty, R. M. Dickson, *J. Am. Chem. Soc.* **2003**, *125*, 7780.
[30] A. Shukla, S. Mukherjee, S. Sharma, V. Agrawal, K.V. Radha Kishan, P. Guptasarma, *Arch. Biochem. Biophys.* **2004**, *428*, 144.
[31] P. Guptasarma, *Arch. Biochem. Biophys.* **2008**, *478*, 127.
[32] N. Goswami, A. Makhal, S. K. Pal, *J. Phys. Chem. B* **2010**, *114*, 15236.
[33] P. Padayatti, G. Palczewska, W. Sun, K. Palczewski, D. Salom, *Biochemistry* **2012**, *51*, 1625.
[34] S. Eustis, M. El-Sayed, *J. Phys. Chem. B* **2005**, *109*, 16350.
[35] E. Dulkeith, T. Niedereichholz, T. A. Klar, J. Feldmann, G. von Plessen, D. I. Gittins, K. S. Mayya, F. Caruso, *Phys. Rev. B* **2004**, *70*, 205424.
[36] M. R. Beversluis, A. Bouhelier, L. Novotny, *Phys. Rev. B* **2003**, *68*, 115433.
[37] M. D. Hughes, Y.-J. Xu, P. Jenkins, P. McMorn, P. Landon, D. I. Enache1, A. F. Carley, G. A. Attard, G. J. Hutchings, F. King, E. H. Stitt, P. Johnston, K. Griffin, C. J. Kiely, *Nature* **2005**, *437*, 1132.
[38] H. Adachi, K. Takano, H. Matsumura, T. Inoue, Y. Mori, T. Sasaki, *J. Synchrotron Radiat.* **2004**, *11*, 121.
[39] O. L. Muskens, S. L. Diedenhofen, M. H. M. van Weert, M. T. Borgström, E. P. A. M. Bakkers, J. G. Rivas, *Adv. Funct. Mater.* **2008**, *18*, 1040.
[40] J. A. Gardecki, M. Maroncelli, *Appl. Spectrosc.* **1998**, *52*, 1179.
[41] D. V. O'Connor, D. Phillips, *Time-correlated Single Photon Counting*, Academic Press, London **1984**.
[42] D. V. O'Connor, W. R. Ware, J. C. Andre, *J. Phys. Chem.* **1979**, *83*, 1333.
[43] J. R. Lakowicz, *Principles of Fluorescence Spectroscopy*, 3rd edition, Springer, New York **2006**.